An Analysis of Stress Distribution in a Spline Shaft Subjected to Cycilc Impulsive Load

Ass. Prof. Dr. Fathi A. AL- Shammaa
Department of Mechanical Engineering
University of Baghdad
E-Mail: Fathi_alshammaa@yahoo.com

Hawaa F. Kadhim
Department of Mechanical Engineering
University of Baghdad
E-Mail: Hawaa_Falih@yahoo.com

ABSTRACT

In this paper the effect of engagement length, number of teeth, amount of applied load, wave propagation time, number of cycles, and initial crack length on the principal stress distribution, velocity of crack propagation, and cyclic crack growth rate in a spline coupling subjected to cyclic torsional impact have been investigated analytically and experimentally. It was found that the stresses induced due to cyclic impact loading are higher than the stresses induced due to impact loading with high percentage depends on the number of cycles and total loading time. Also increasing the engagement length and the number of teeth reduces the principal stresses (40%) and (25%) respectively for increasing the engagement length from (0.15 to 0.23) and the number of teeth from (8 to 10). while increasing the other parameters (amount of applied load, wave propagation time, number of cycles, and initial crack length) increase the principal stresses at the root of the tooth (37% when the applied load rises from (8 KN to 11KN) and (62% when the wave propagation time rises from (0.5 to 1).

Key words: spline coupling, cyclic impact, stress distribution, velocity of crack propagation, cyclic crack growth rate.

الخلاصة

في هذا البحث تم اجراء دراسة عملية ونظرية لتأثير طول التعشيق, عدد الاسنان, مقدار الحمل المسلط, زمن انتقال الموجة, عدد الدورات, والطول الابتدائي للشق على كل من توزيع الاجهادات الرئيسية, سرعة امتداد الشق, و معدل نمو الشق الدوري في وصلة اللربط المسننة المعرضة لصدمة دورية التوائية. وقد وجد ان الاجهادات الرئيسية الناتجة عن الصدمة الدورية اعلى من الاجهادات الرئيسية الناتجة عن صدمة منفردة بنسبة عالية تعتمد على عدد الدورات و زمن التحميل. وان زيادة طول التعشيق وعدد الاسنان يقلل الاجهادات المتولدة بنسبة(40% 25%)على التوالي عند زيادة طول التعشيق من (0.15m الى 0.23m)وعدد الاسنان من(8 الى10)في حين زيادة العوامل الاخرى (مقدار الحمل المسلط, زمن انتقال الموجة, عدد الدورات, والطول الابتدائي للشق) تؤدي الى زيادة الاجهادات الرئيسية المتولدة في وصلة الربط المسننة.حيث يزداد(37%)عند زيادة الحمل المسلط من(8 الى 11KN) و(62%)عند زيادة زمن انتقال الموجة من (0.5 الى 1).

1.INTRODUCTION

A spline coupling is an effective mode of torque transfer between two rotating parts. It transmits torque, but permits axial sliding. The spline coupling is used in high torque transmission engines like vehicles, turbines, and jet engines. The literature that deals with spline coupling has been investigated experimentally and theoretically in several studies which considered the spline tooth profile like ; **Yeung 1999, Baker 1999, Chitkara et al 2001,** and **Yang et al 2007**, failure analysis of the spline coupling like: **Li et al 2007, Ding et al 2007, Ding et al 2008,** and **Lin et al2008**, and the stress distribution along the axial direction of a spline coupling under static load like; **Taylor 2001, Tjernberg 2001, Barrot et al 2009, and Grath 2009**. In the present work the stress distribution, velocity of crack propagation, and cyclic crack growth rate in a spline coupling

subjected to cyclic torsional impact load have been investigated analytically and experimentally for two different boundary conditions.

2.ANALYTICAL ANALYSIS

The torque distribution along the pressure face of the spline coupling tooth was assumed to be unevenly distributed due to the deformation occurs in the spline teeth which caused during torque transmitting ,**Baker 1999**, see **Fig. 1.**

For a spline coupling subjected to impact load the torque distribution along the axial direction can be described as; **Barrot 2009**.

$$m(x) = N\,R\,C\,P(x) = c_\theta[\theta_1(x) - \theta_2(x)] \quad (1)$$

Where;

$$\alpha = \sqrt{[\frac{C_{\theta 2}}{G_2 J_2} + \frac{C_{\theta 1}}{G_1 J_1}]} \quad (2)$$

$$J_1 = \frac{\pi\,(D_0^4 - D_i^4)}{32} - \left(N\frac{C\,w^3}{12} + N\frac{w\,C^3}{12}\right) \quad (3)$$

$$J_2 = \frac{\pi\,D_i^{\,4}}{32} + \left(N\frac{C\,w^3}{12} + N\frac{w\,C^3}{12}\right) \quad (4)$$

$$C_\theta = \frac{T\,J}{L\,R} \quad (5)$$

The coefficients A and B depend on the boundary condition of the spline coupling. Two types of boundary conditions were studied, in the first type the spline shaft was fixed (built in) at one end and free at the other and the sleeve was engaged at the free end, so it called (Built in-Free spline coupling BFSC). In the second type the spline shaft was fixed at both ends and the sleeve was engaged at the middle of the shaft and it was called (Built in-Built in spline coupling BBSC).

For (BFSC); m (0, t) =0 , m (L, t) =T

$$A = \left[\frac{T}{e^{\alpha L} - e^{-\alpha L}}\right] \quad (6)$$

$$B = \left[\frac{-T}{e^{\alpha L} - e^{-\alpha L}}\right] \quad (7)$$

For (BBSC); m (0, t) =T , m (L, t) =T

$$A = T\left[\frac{e^{\alpha L} - 1}{e^{2\alpha L} - 1}\right] \quad (8)$$

$$B = T\left[\frac{e^{2\alpha L} - e^{\alpha L}}{e^{2\alpha L} - 1}\right] \quad (9)$$

The torque transmitted due to cyclic impact load was described as follows;

$$m(x,t)_{cyclic} = [Ae^{\alpha x} + Be^{-\alpha x}]\left[e^{\frac{t}{t_o}} - 1\right]\left[f\frac{t}{t_o}\right] \qquad (10)$$

3. PRINCIPAL STRESS DISTRIBUTION

The principal stress distribution was calculated using the equation ; **Mancuso, J.R.,2001**

$$\sigma_1(x,t) = \frac{m(x,t)}{N\,R\,C\,L} \qquad (11)$$

$$\sigma_1(x,t)_{cyclic} = \frac{m(x,t)_{cyclic}}{NR\,C\,L} \qquad (12)$$

4. VELOCITY OF CRACK PROPAGATION

As the crack propagates the displacement V will change with time. Denoting the rate of change dV/dt as V'; **Ewalds, 1989**.

$$V' = \frac{Z_1}{E^{\circ}}[\,\sigma\,a' + \sigma' a] \qquad (13)$$

$$V' = \frac{Z_1}{E^{\circ}NCRL}\left[\left[[Ae^{\alpha x} + Be^{-\alpha x}]\left[e^{\frac{t}{t_o}} - 1\right][f\frac{t}{t_o}]\sqrt{\frac{\pi}{k}}\sqrt{\frac{E^{\circ}}{\rho}}\left(1 - \frac{a_o}{a_i}\right)\right] + [[Ae^{\alpha x} + Be^{-\alpha x}][\left[\left[e^{\frac{t}{t_o}} - 1\right]\frac{f}{t_o}\right] + \left[\left[\frac{1}{t_o}e^{\frac{t}{t_o}}\right]f\frac{t}{t_o}\right]]a\right] \qquad (14)$$

Where;

$$a' = \sqrt{\frac{\pi}{k}}\sqrt{\frac{E^{\circ}}{\rho}}\left(1 - \frac{a_o}{a_i}\right) \qquad (15)$$

$$E^{\circ} = E/(1 - v^2)$$

$$Z_1 = 2\sqrt{a^2(1 - z^2)} \qquad (16)$$

$0 < z < 1$

For steel $\sqrt{\frac{\pi}{k}} = 0.8$

5. CYCLIC CRACK GROWTH RATE

Paris' law relates the stress intensity factor rang to sub-critical crack growth rate. The basic formula reads;

$$\frac{da}{dn} = C_2 \Delta K^m \qquad (17)$$

The term in the left hand side known as the crack growth rate under cyclic loading regime is called cyclic crack growth rate. On the right hand side C_2 and **m** are material constants, and **ΔK** is the range of the stress intensity factor.

$$\Delta K = K_{max} - K_{min} \quad (18)$$

$$\Delta K = \Delta\sigma Y\sqrt{\pi a} \quad (19)$$

For an edge crack in an infinite sheet **Y=1.12, Ewalds, 1989.**

For steel **m=3** and C_2**is** 10^{-11}, **David R., 2001**, see **Fig.2.**

6. EXPERIMENTAL WORK

A spline coupling models of ST-45 simulate the spline coupling of a Power Take-Off engine have been manufactured at the manufactory of "THE STATE COMPANY OF MECHANICAL INDUSTRES" with two number of teeth (8 and 10) and three engagement lengths (0.08m,0.15m,0.23m). The spline coupling samples were manufactured in two groups the first group suitable to set as (BBSC) and the second group suitable to set as (BFSC). The test rig consisted of fixing plate which is a heavy rectangular base with two vertical plates. At the upper end of each vertical plate there is a circular hole to carry and fix the spline coupling samples. The impactor which consisted of two arms connected to a disc. The disc had a several holes around its circumference each hole represented a different winding angle which causes a different amount of load. The disc was connected to a helical spring, see **Fig. 3**. The strain induced at the root of the spline coupling tooth was measured using strain gauges connected to a sensor circuit to convert the change in resistance into change in voltage and amplify the strain gauge output signal. The output signal of the sensor circuit goes to a digital data logger, (ORDEL UNIVERSAL DATA LOGGER (UDL 100)), to record the data and the display and save them on a computer, see **Fig. 4**.

7. ANALYTICAL RESULTS

Theoretical investigation is done for two loading cases (impact load and cyclic impact load), two boundary conditions (BBSC and BFSC), three engagement lengths (0.08m,0.15m,0.23m), and three amounts of applied load (5 kN, 8 kN, 11 kN). **Fig. 5** shows that the principal stress distributes exponentially along the axial direction of the BFSC tooth and that the principal stresses induced in the spline shaft are higher than the principal stresses induced in the sleeve because of the difference between their geometry especially their root radiuses. **Fig. 6** shows that the principal stress distributes exponentially along the axial direction of the BBSC tooth and it distributes evenly due to the symmetric boundary conditions at its both ends. **Fig. 7** shows that the principal stresses induced due to applying cyclic impact load are higher than the principal stresses induced due to applying impact load with high different percentage depends on the number of cycles per unit time and the total loading time. The increasing in stresses results from accumulating the stresses induced at each cycle. **Fig. 8** shows that increasing the amount of the applied load increases the induced principal stresses and the increasing is linear because the stresses are linearly related to the amount of applied load. **Fig. 9** shows the significant effect of the engagement length on the principal stresses where it shows that increasing the engagement length reduces the principal stresses with a high ratio due to increasing the area that carries the load. **Fig. 10** shows that increasing the number of teeth reduces the induced principal stresses due to dividing the applied load on a higher number of teeth and hence each tooth carries fewer load. **Fig. 11** shows that the principal stresses increases exponentially with the wave propagation time and 62% of this increasing occurs between (t/to =0.5 to t/to =1). **Fig. 12** shows that the behavior of the velocity of crack propagation is similar to the behavior of the principal stresses with respect to time. That is because the velocity of crack propagation depends on the principal stress values. Also **Fig.12** shows that increasing the number of cycles increases the velocity of crack propagation due to increasing the accumulated stresses. **Fig. 13** shows that the cyclic crack growth rate increases with increasing the number of cycles, this

increasing occurs due to increasing the accumulative stresses from each cycle. **Fig. 14** shows that the cyclic crack growth rate increases with high percentage with increasing the initial crack length because of increasing the energy released from the tooth. The energy released causes energy concentration at the tip of the crack which results in increasing the principal stresses at the tip of the crack that's results in increasing the cyclic crack growth rate.

8. EXPERIMENTAL RESULTS

Fig. 15 shows that increasing the amount of the applied load increases the induced principal stresses and this increasing is linear. **Fig. 16** shows that at the fixed end of the spline coupling the effect of the amount of the applied load on the induced principal stresses is the same for (BBSC) and (BFSC). **Fig. 17** shows that increasing the number of the spline coupling teeth reduces the induced principal stresses due to distribute the load over a higher number of teeth hence each tooth carries less load. **Fig. 18** shows that increasing the engagement length have a significant effect in reducing the induced principal stress because of increasing the area carries the load. **Fig. 19** shows that the stresses induced due to cyclic impact load are higher than the stresses induced due to impact load with a high percentage depends on the number of cycles per unit time and the total loading time. **Fig. 20** shows that increasing the number of cycles results in increasing the velocity of crack propagation due to increasing the accumulative stresses that accumulates from each cycle. **Fig. 21** shows that the cyclic crack growth rate increases exponentially with the increasing of the number of cycles, this increasing occurs due to the increasing of the accumulative stresses.

9. VERIFACATION

The experimental results verified the theoretical results and showed a good agreement with reasonable error percentage comes from the delay time of the response of the measuring instruments therefore this error percentages increase as the impact wave propagates faster due to increasing the delay time. **Fig. 22** shows that the experimental results of the principal stress variation with the amount of applied load coincides with the theoretical results with an error percentage equals to (9%). **Fig. 23** shows that the experimental results of the velocity of crack propagation variation with the wave propagation time coincides with the theoretical results with an error percentage equals to (9%). **Fig. 24** shows that the experimental results of the cyclic crack growth rate variation with the number of cycles coincides with the theoretical results with an error percentage equals to (10%).

10. CONCULUSIONS

1. The principal stresses induced in the spline shaft are different from the principal stresses induced in the sleeve with a percentage depends on their geometry.
2. The end of the engagement length endures the maximum stress and it's the most susceptible point to failure.
3. In the BBSC both ends endures the maximum stresses while in the BFSC only one end endures the maximum stresses.
4. The engagement length has a significant effect on reducing the stresses**.**
5. The time of wave propagation of the cycling impact loads wave have a very significant effect on the stresses induced in the spline shaft then the impact loads**.**
6. Appling cyclic impact load on the spline coupling highly raises the velocity of crack propagation.
7. The cyclic growth rate obeys Paris law.

NOMENCLUTURE

Symbol	meaning	Unit
A:	coefficient	#
B:	coefficient	#
C :	spline tooth height	Mm
N :	number of teeth	#
L:	engagement lengt	mm
W:	spline tooth width	mm
w :	applied load	applied load
X:	axial posision	mm
m:	material coefficient	#
.n:	number of cycles	Cpm
Z :	half crack length	mm
k:	integral constant	#
K:	stress intensity factor	Mpa
T:	applied torque	KN.m
t:	instantaneous wave propagation time	Sec
t_o:	total wave propagation time	Sec
E :	modulus of elasticity	Kn.m
Cpm:	cycle per minute	cycle/min
G:	modulus of rigidity	KN.m
a:	crack length	mm
a_o:	Initial crack length	mm
a_i :	instantaneous crack length	mm
C_2:	material coefficient	#
R_1:	sleeve root radius	mm
R_2:	shaft root radius	mm
R_o :	sleeve outer radius	mm
R_p:	spline coupling pitch radius	mm
J_1:	sleeve polar moment of inertia	mm^4
J_2:	shaft polar moment of inertia	mm^4
P(x):	static presser	Kpa
$M_1(x,t)$:	torque transmitted by sleeve	Kn.m
$M_2(x,t)$:	Torque transmitted by shaft	Kn.m
m(x,t):	torque transmitted by	Kn.m
$m(x,t)_{cyclic}$	transmitted torque	Kn.m
Kn.m:	Spline coupling	due to cyclic impact load
V:	velocity of crack propagation	m/sec
V'_i:	impact velocity of crack	m/sec`
α:	coefficient	N/rad
ρ:	material density	Kg/m^3
v:	poison's ratio	#
$\sigma_1(x,t)$:	principal stress	KN/m^2
C_θ:	torsional rigidity	KN/rad

$\sigma_1(x,t)_{cyclic}$	principal stress due to	cyclic impact load
θ_1:	sleeve angle of twist	rad
θ_2:	shaft angle of twist	rad

REFERANCES

Ali, M.A., 2009,*A Study of a Delimitation Problem in a Leaf Spring Made of Composite Material under Impact Load*, M.Sc. Thesis, University of Baghdad, Baghdad.

Baker, D.A, 1999, *A Finite Element Study of Stresses in Stepped Spline Shafts and Partially Splined Shafts under Bending, Torsion And Combined Loadings*", M.Sc. Thesis, Virginia Polytechnic Institute , State University, Virginia.

Barrot, A., Paredes, M., and Sartor. 2009, *Extended Equations of Load Distribution in the Axial Direction in a Spline Coupling*, Journal of Engineering Failure Analysis, Vol. 16, P.P. 200-211.

Darrell, F.S., and Gary, B.M., 2000,*Multiaxial Fatigue*, SAE,Inc.

David, Roylance, 2001,, *Fatigu*e, Department of Materials Science and Engineering, Massachusetts Institute of Technology, Cambridge, MA 02139.

Ding, J., Leen, S.B., Williams, E.J., and Shipway, P.H., 2008, *Finite Element Simulation of Fretting Wear-Fatigue Interaction in Spline Couplings*, Journal of Tribology, Vol.2, No. (1).

Ding, J., McColl, I.R., Leen, and S.B., 2007, *The Application of Fretting Wear Modeling To a Spline Coupling*, Journal of Wear,Vol.262, P.P.1205-1216.

Ewalds, H.L., and Wanhill, R.J.H. 1989, *Fracture Mechanics*, Edward Arnold.

Grath, J.P., 2009, *Analysis of Axial Load Distribution in a Jet Engine Disk-Shaft Spline Coupling*, M.Sc. Thesis, Faculty of Rensselaer Polytechnic Institute.

Hall, A.S., Holowenko, A.R., and Laughlin, H.G., 1961, *Theory and Problems of Machine Design*, Schaum's outline, Mc-Graw Hill, Inc.

Hearn, E.J., 2000, *Mechanics of Materials1*, Butterworth Heinemann.

Johanson, W. 1972, *Impact Strength of Materials*, Edward Arnold.

Jonas, A.Z., Theodore, N., Hallock, F.S., Longin, B.G., and Donald, R.C., 1982, *Impact Dynamics*, John Wiley &Sons.

Li, Y.J., Zhang, W.F., and Tao, C.H., 2007, *Fracture Analysis of Castellated Shaft* Journal of Engineering Failure Analysis, Vol.14, P.P.573-578.

Lin, C., Hung, J., and Hsu, T., 2008, *Failure Analysis of Reverse Shaft in the Transmission System of All-Terrain Vehicles*, Journal of Fail. Anal. and Prevent. , Vol. 8, P.P. 75-80.

Mancuso, J.R., and Jones, R., 2001, *Coupling Interface Connection*

Naser Shabakhty, 2004, *Durable Reliability of Jack-up Platforms*, Ph.D. Thesis, Delft University of Technology, Netherlands.

Sowrappa, L.R., 2005, *Laminated Architecture Glass Subjected to Blast, Impact loading,*

Patricio, M., and Mattheji, R.M.M., 2002, *Crack Propagation Analysis*.

Shigly, 2006,*Mechanical Engineering Design,* Mc-Grow Hill Inc., eighth edition.

Tariq, M.H., 2008,*The Effect of Low Velocity Impact with Fatigue Loading on Cracked Rectangular Plate* M.Sc. Thesis, University of Baghdad, Baghdad.

Taylor, J.W., 2001, *Modeling and Simulation of Spline Couplings*, United Kingdom.

Tjernberg, A., 2001, *Load Distribution and Pitch Errors in a Spline Coupling*, Journal of Materials and Design, Vol.22, P.P.259-266.

Varin, J.D., 2002,*Fracture Characteristic of Steering Gear Sector Shaft*, Journal of Practical Failure Analysis, Vol.2, No.(4), P.P.65-69.

Yang, D.C.H., and Tong, s., 2007, *On the Profile Design of Transmission Splines and Keys* Journal of Mechanism and Machine Theory, Vol.42, P.P.82-87.

Yeung, K.S., 1999, *Analysis of a New Concept in Spline Design for Transmission Output Shafts*", Ford Motor Company, Dearborn, MI, 24121, USA.

http://en.wikipedia.org/wiki/Paris'_law
http://en.wikipedia.org/wiki/Spline-(mechanical)
http://www.facebook.com/pages/Rotating-spline/143902598956699?sk=wiki

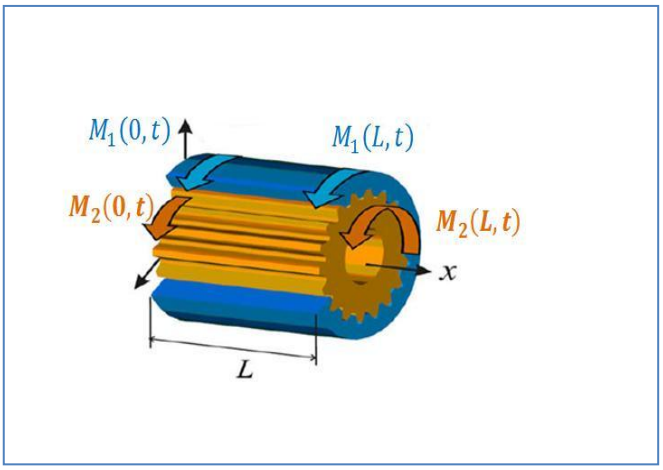

Figure 1. Schematic figure of the spline coupling.

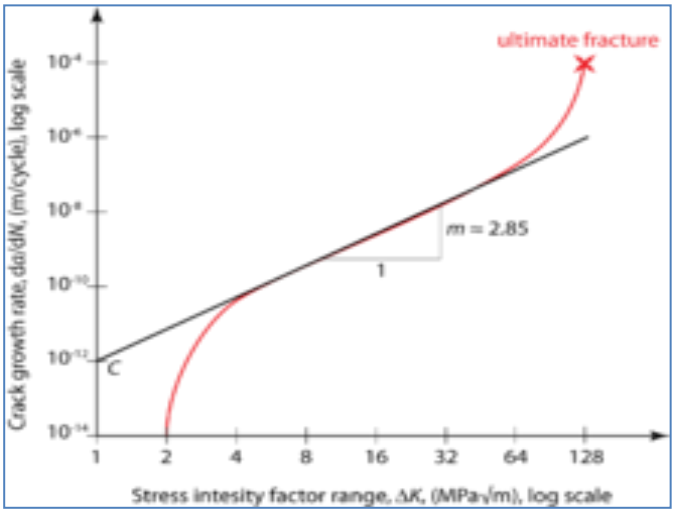

Figure 2. Schematic plot of the typical relationship between the crack growth rate and the range of the stress intensity.

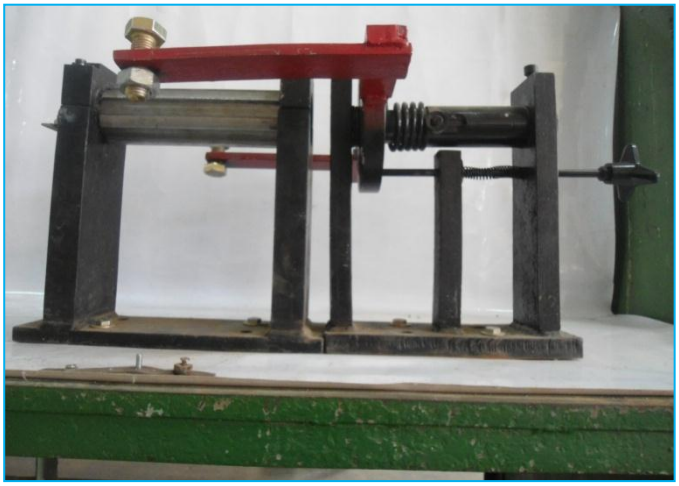

Figure 3. The fixing plate and the impact.

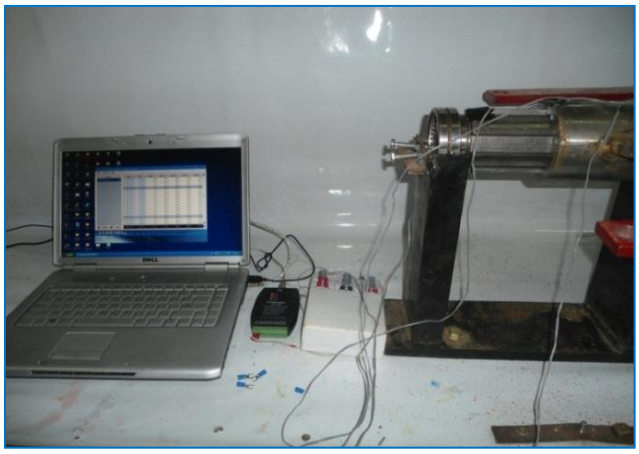

Figure 4. The measuring instruments.

.

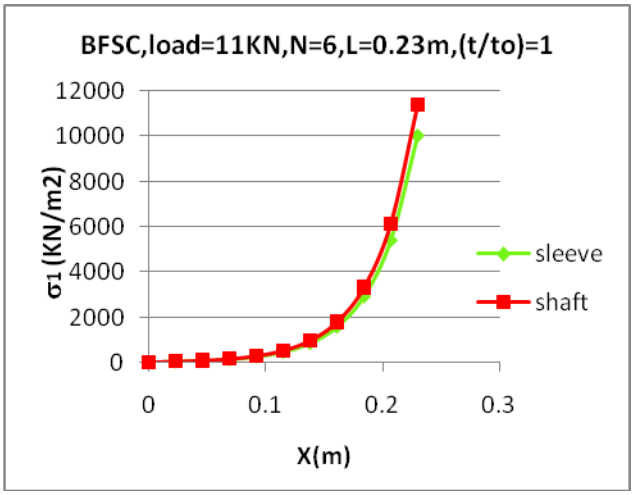

Figure 5. Principal stress distribution along the axial direction of a (bfsc) tooth due to impact load.

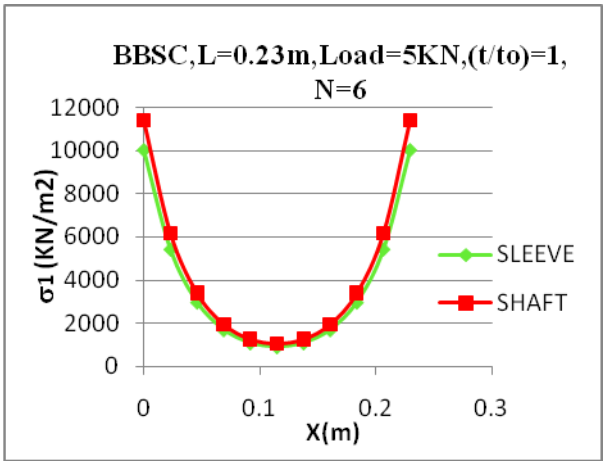

Figure 6. Principal stress distribution along a (bbsc).

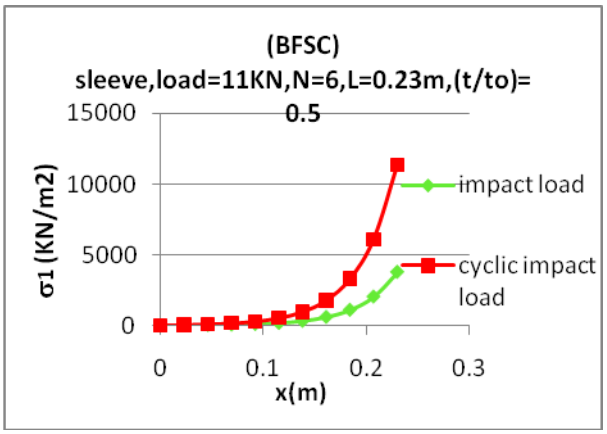

Figure 7. Effect of cyclic impact load on the principal stress values.

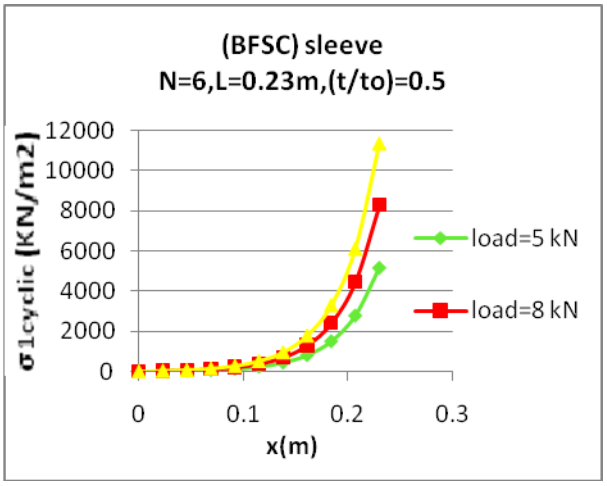

Figure 8. Principal Stress Distribution along a (BFSC) Sleeve for 3 Different Cyclic Loads.

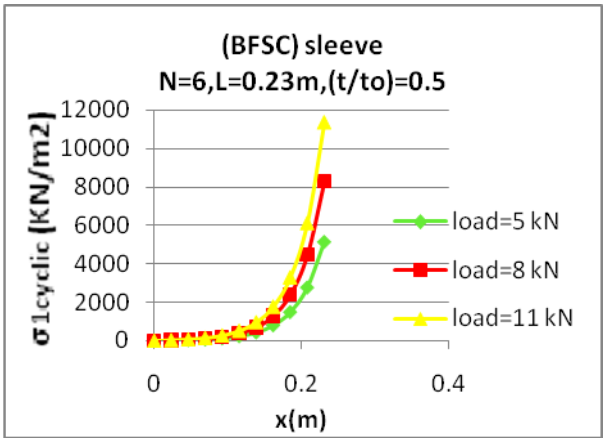

Figure 9. Principal stress distribution along a (bfsc) sleeve for 3 different cyclic loads.

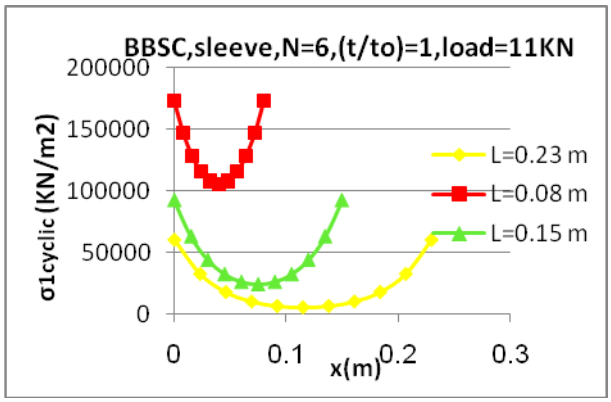

Figure 10. Stress distribution along a (bbsc) sleeve for 3 different engagement lengths.

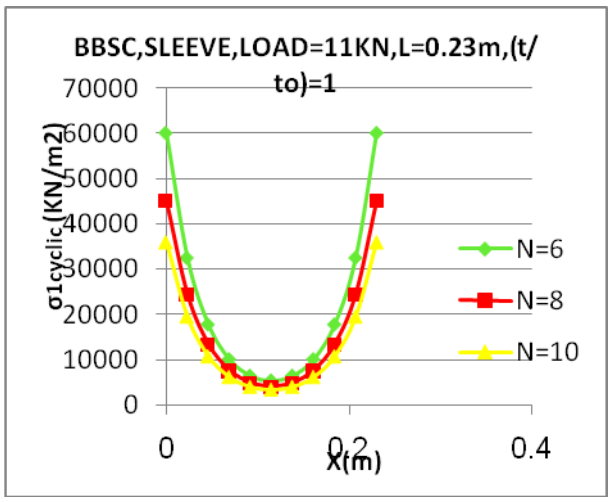

Figure 11. Stress distribution along a (bbsc) sleeve for 3 different numbers of teeth.

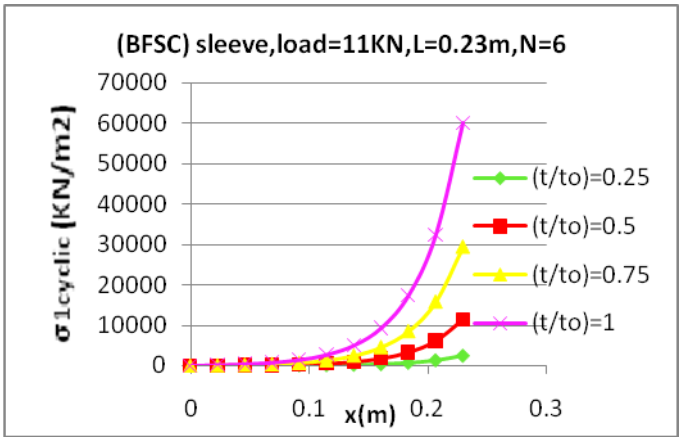

Figure 12. Stress distribution along a (bfsc) sleeve at 4 different wave propagation times.

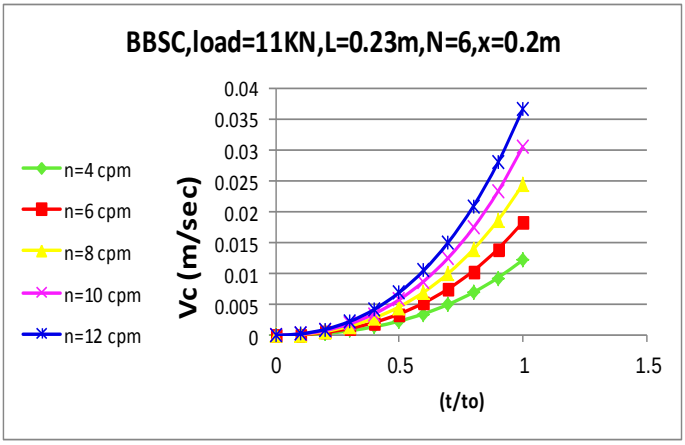

Figure 13. Velocity of crack propagation due to cyclic impact load for 5 different numbers of cycles.

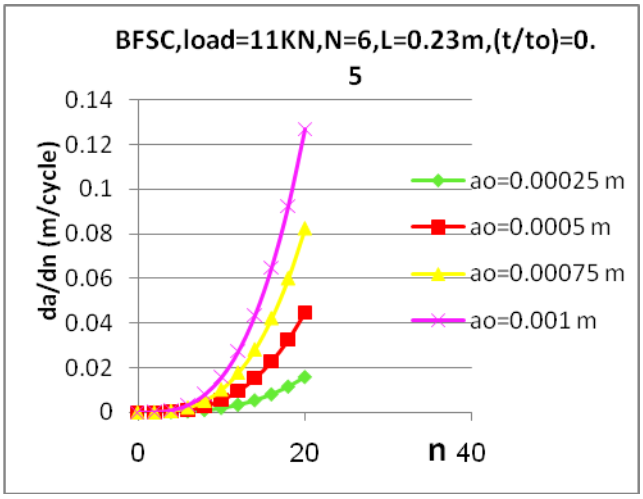

Figure 14. Cyclic crack growth rate variation with number of cycles.

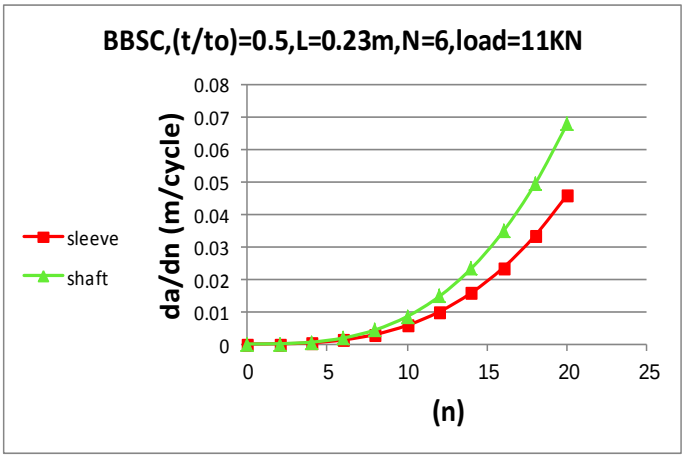

Figure 15. Cyclic crack growth rate for 4 different initial crack lengths.

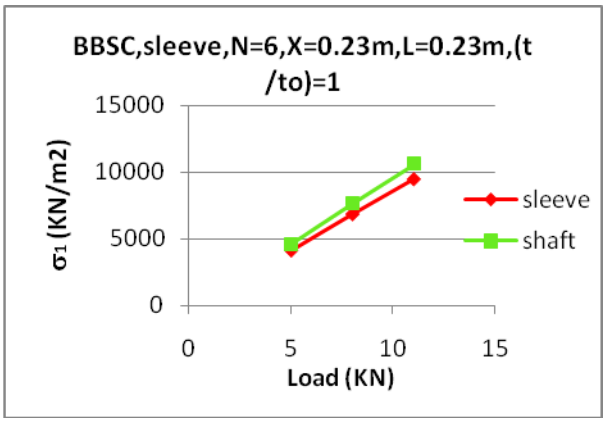

Figure 16. Principal stress variation with amount of applied load.

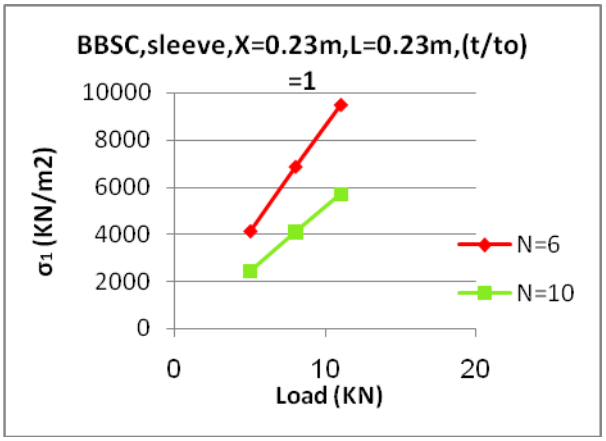

Figure 17. Principal stress variation with the amount of applied load for 2 different number of teeth.

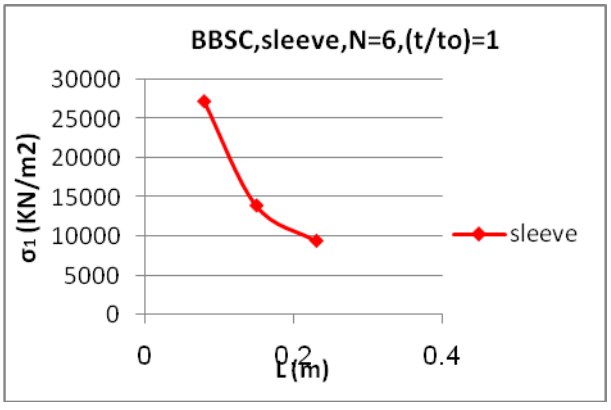

Figure 18. Principal stress variation with the engagement length.

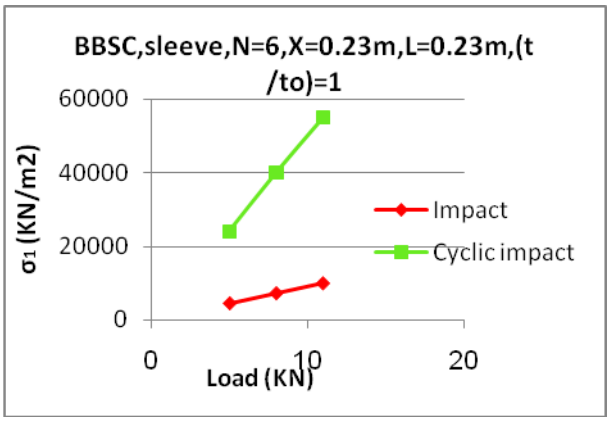

Figure 19. Principal stress variation with the amount of applied load for impact and cyclic impact load.

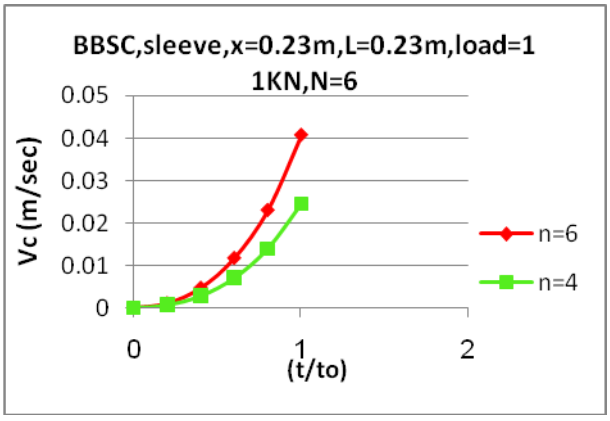

Figure 20. Variation of velocity of crack propagation with wave propagation time for 2 different numbers of cycles.

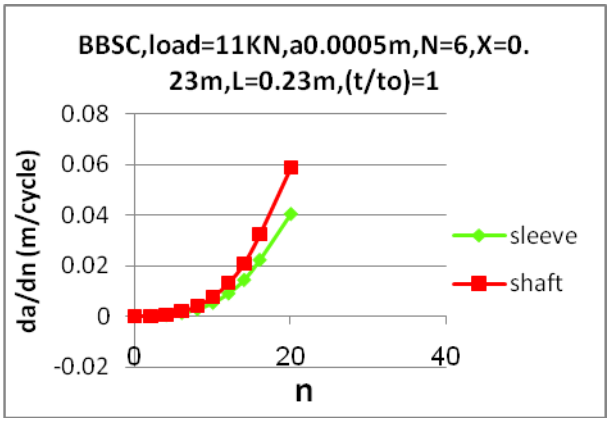

Figure 21. Cyclic crack growth rate variation with the number of cycles.

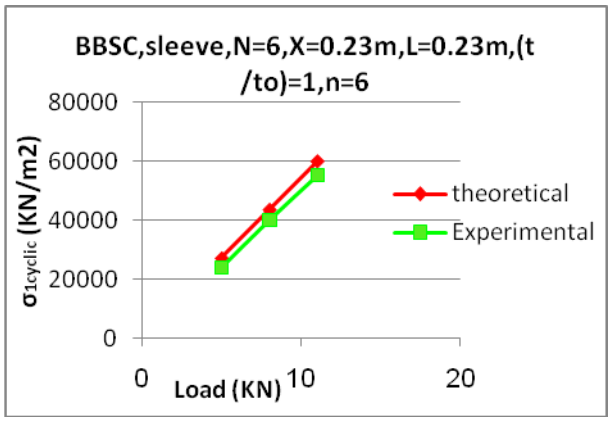

Figure 22. Comparison between the experimental and theoretical results for the principal stress variation with the amount of cyclic impact load.

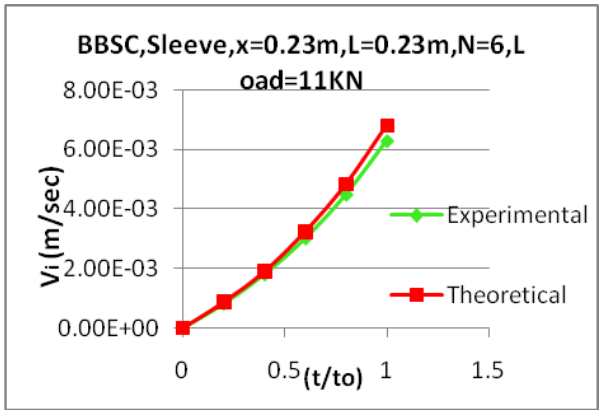

Figure 23. Comparison between the experimental and theoretical results of velocity of crack propagation variation with the wave propagation time**.**

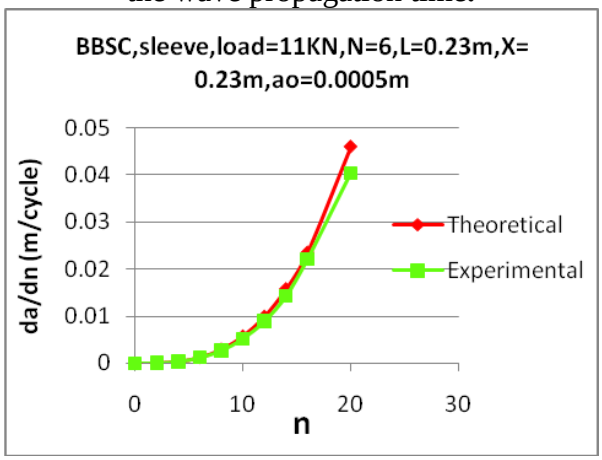

Figure 24. Comparison between the experimental and theoretical results of the cyclic crack growth rate variation with the number of cycles.